Learning based super-resolution land cover mapping

Feng Ling, Yihang Zhang, Giles M. Foody *IEEE Fellow*, Xiaodong Li,

Xiuhua Zhang, Shiming Fang, Wenbo Li, Yun Du

F. Ling, Y. Zhang, X. Li, and Y. Du are with the Key Laboratory of Monitoring and Estimate for Environment and Disaster of Hubei Province, Institute of Geodesy and Geophysics, Chinese Academy of Sciences, Wuhan 430077, China (e-mail: lingf@whigg.ac.cn).

G. M. Foody is with the School of Geography, University of Nottingham, University Park, Nottingham NG7 2RD, UK

X. Zhang is with the Wuhan Institute of Technology, Wuhan 430205, China

S. Fang is with the School of Public Administration, China University of Geosciences, Wuhan 430074, China.

W. Li is with the Hefei Institute of Technology Innovation, Chinese Academy of Sciences, Hefei, 230088, China.

[*]Corresponding author: lingf@whigg.ac.cn

Abstract: Super-resolution mapping (SRM) is a technique for generating a fine spatial resolution land cover map from coarse spatial resolution fraction images estimated by soft classification. The prior model used to describe the fine spatial resolution land cover pattern is a key issue in SRM. Here, a novel learning based SRM algorithm, whose prior model is learned from other available fine spatial resolution land cover maps, is proposed. The approach is based on the assumption that the spatial arrangement of the land cover components for mixed pixel patches with similar fractions is often similar. The proposed SRM algorithm produces a learning database that includes a large number of patch pairs for which there is a fine and coarse spatial resolution representation for the same area. From the learning database, patch pairs that have similar coarse spatial resolution patches as those in input fraction images are selected. Fine spatial resolution patches in these selected patch pairs are then used to estimate the latent fine spatial resolution land cover map, by solving an optimization problem. The approach is illustrated by comparison against state-of-the-art SRM methods using land cover map subsets generated from the USA's National Land Cover Database. Results show that the proposed SRM algorithm better maintains the spatial pattern of land covers for a range of different landscapes. The proposed SRM algorithm has the highest overall accuracy and Kappa values in all these SRM algorithms, by using the entire maps in the accuracy assessment.

Index Terms：Super-resolution mapping; Learning database; Patch pairs; Neighboring patches

I. Introduction

Super-resolution mapping (SRM), which is also referred to sub-pixel mapping, is a method to generate fine spatial resolution land cover maps from coarse spatial resolution remote sensing images. SRM can be viewed as the post-processing of soft classification to further address the mixed pixel problem that is common in coarse spatial resolution images [1, 2]. In general, soft classification estimates the fraction images that illustrate the area percentage cover of land cover classes within coarse spatial resolution mixed pixels. The fraction images may be input to a SRM analysis to predict the spatial locations of the land cover class at a fine spatial resolution. The output of the SRM analysis is a hard classification land cover map, which has a finer spatial resolution than that of input fraction images. At present, SRM has become a promising method to reduce the mixed pixel problem that is widely encountered with coarse spatial resolution images, and has been successfully used in many applications, such as mapping waterlines [3-5], lakes [6], urban buildings [7], urban trees [8], forests [9], as well as in ground control point refinement [10] and the calculation of landscape pattern indices [11].

A large number of SRM algorithms have been proposed [12-27]. Generally, SRM is an ill-posed problem [28], and the prior information about the spatial pattern of different land cover classes at the fine spatial resolution scale needs be known before SRM is performed. Therefore, in order to estimate the latent fine spatial resolution land cover map from input coarse spatial resolution fraction images, one of the key issues is the definition of the prior model. The latter has been described from different perspectives. In the simplest case, when only the coarse spatial resolution fraction images are available, the prior model is often based on the spatial dependence principle, which aims to make the fine spatial resolution land cover map have the maximal spatial dependence [1]. In practice, the spatial dependence of a certain fine spatial resolution pixel can be calculated by comparing it with its neighboring fine spatial resolution pixels [14], fractions of its neighboring coarse spatial resolution pixels [29], or both of them [30]. Moreover, anisotropic land cover dependences have also been

proposed to describe the spatial land cover pattern more precisely [31], especially for some special land cover classes [7, 32]. The spatial dependence model is a popular model for use in SRM due to its simplicity and absence of requirements for additional information about the spatial pattern of the land cover. However, the model can be inappropriate for areas with complex land cover patterns. The use of the wrong prior model in a SRM analysis can result in an inappropriate and inaccurate land cover representation, possibly even worse than that of a standard hard classification of the coarse resolution image in some cases [6, 33].

A promising approach to improve the effectiveness of the prior model is through the incorporation of additional information on the land cover to inform the SRM analysis. Various approaches have been used. An intuitive additional dataset to use in a SRM analysis is another kind of fine spatial resolution images, such as a panchromatic band image [34-37] or a fine spatial resolution synthetic aperture radar (SAR) image [38]. Fine spatial resolution digital elevation model [4, 5] and light detection and ranging (LIDAR) data [39], and vector datasets [40] have also been successfully used to refine SRM analyses. Multiple sub-pixel shifted coarse spatial resolution images which are used as an alternation datasets to provide additional information about the spatial land cover pattern [41] for SRM, and this method has been further developed [6, 42-45]. A historical fine spatial resolution land cover map can also be used to help the SRM analysis [9, 46, 47]. Adding site-specific additional datasets can increase the accuracy of SRM, however, this kind of approach is often limited because the additional dataset should cover the same area, in its entirety, as the input fraction images, and this may often not be the case with the additional data only available for part of the region being mapped.

In addition to the aforementioned approaches, the spatial land cover pattern can also be learned from the training image, which is often a fine spatial resolution land cover map that has a similar spatial land cover pattern to the objective fine spatial resolution land cover map. In this situation, SRM predicts the fine spatial resolution land cover map from input coarse spatial resolution fraction images with the aid of the prior model

that is learned from these training fine spatial resolution land cover maps. One kind of learning based SRM algorithm uses a model to describe the fine spatial resolution land cover pattern, and the parameters of the prior model are learned from the training maps [48-50]. Central to this kind of approach is the selection of the prior model. Presently, a popular approach is to use a semi-variogram based approach in which the SRM aims to produce a fine spatial resolution land cover map that has the same spatial pattern as that represented by the semi-variogram fitted to the available fine spatial resolution land cover map. A critical drawback of this category of SRM algorithms is, however, that the geo-statistical methodologies are constructed based on the assumption of spatial stationary, and they are limited for complex land cover patterns which are often non-stationary.

Another kind of learning based SRM algorithms directly learns the relationship between coarse spatial resolution fraction images and the fine spatial resolution land cover maps without a predefined model [51-54]. The basic assumption of this method is that the fine spatial resolution spatial land cover pattern is similar for a mixed pixel patch, which is basically a block of coarse resolution pixels, with similar land cover class fractional composition. Several algorithms have been proposed to learn the relationship, including the back-propagation (BP) neural networks [51-54], and the support vector regression algorithms [55]. The SRM algorithms belonging to this category often include two steps. In the first step, a fine spatial resolution image is estimated for each land cover class using the learned relationship. In the second step, fine spatial resolution pixel labels are assigned with the maximum *a posteriori* principle using all of these estimated fine spatial resolution images and input fraction images as constraints. This kind of learning based SRM algorithm are special cases of the interpolation-based SRM algorithm [56]; only the interpolation step is performed by the learning based methods. As a result, the limitation of the interpolation-based SRM algorithm, notably salt-and-pepper and linear artifacts, is unavoidable for this category of learning based SRM algorithm.

In this paper, we propose a novel SRM algorithm, which is also based on the assumption that coarse spatial

resolution mixed pixel patches with similar fractions have a similar fine spatial resolution land cover pattern. Different to other learning based SRM algorithms, the novelty of the proposed learning based SRM algorithm lies in the way the coarse spatial resolution and fine spatial resolution patches are used within the analysis. The proposed method does not need the additional label assignment step and patch outliers are effectively addressed during the analysis, avoiding commonly encountered error sources in other two-step learning based SRM algorithms. The remainder of this paper is organized as follows. Section II details the proposed learning based SRM algorithm. Section III validates the performance of the proposed algorithm through several experiments. Section IV discusses some issues about the proposed algorithm and Section V concludes this paper.

II. Methods

A. Problem description

Suppose that the original coarse spatial resolution remotely sensed image has $M \times N$ pixels and the number of land cover classes in the whole image is C. It is assumed that the fraction images F for all classes have been estimated by soft classification. The SRM analysis aims to generate a fine spatial resolution land cover map H using F as input. By setting the zoom factor to be z, each coarse spatial resolution pixel is divided into $z \times z$ fine spatial resolution pixels. All fine spatial resolution pixels are considered to be pure pixels and each one should be assigned to a single land cover class. The resulting fine spatial resolution land cover map thus contains $(z \times M) \times (z \times N)$ pixels, whose labels are defined to a unique class of C.

In this paper, it is assumed that fraction images F are exactly estimated without error. In each coarse spatial resolution pixel V, the number of fine spatial resolution pixels $Q_c(V)$ assigned to the class $c \in (1, 2, L, C)$ is computed according to the equation:

$$Q_c(V) = \text{round}(f_{F,c}(V) \times z^2) \tag{1}$$

where $f_{F,c}(V)$ is the fractional abundance of the class c within the area represented by the coarse spatial

resolution pixel V in the fraction images F, $\text{round}(x)$ returns the value of the closest integer to x. In this situation, the objective of the SRM analysis is to arrange these fine spatial resolution pixels within each coarse spatial resolution pixel to make the fine spatial resolution land cover map honor a pre-defined spatial pattern model.

For the proposed learning-based SRM algorithm, it is assumed that there are a set of fine spatial resolution land cover maps available. These fine spatial resolution maps could be historical land cover maps or land cover maps derived from fine spatial resolution remote sensing images. These available fine spatial resolution land cover maps are used to provide information about the spatial land cover patterns at the fine spatial resolution. Then, assuming that a mixed pixel patch with similar fractions has similar spatial land cover pattern, the SRM analysis may yield a fine spatial resolution map.

B. The fine and coarse spatial resolution patch pair

For the land cover class c, the spatial land cover pattern is represented by the patch pair $[x_c, y_c]$, in which y_c is a coarse spatial resolution patch and its corresponding fine spatial resolution patch is x_c. Here, square patches of size p are used with a coarse spatial resolution patch including $p \times p$ coarse spatial resolution pixels. The coarse spatial resolution patch is represented by the vector $y_c = [f_c(1), f_c(2), L, f_c(p \times p)]$, where $f_c(V)$ is the fraction value of the coarse spatial resolution pixel V of the class c. The corresponding fine spatial resolution patch includes $z \times p \times z \times p$ fine spatial resolution pixels, and is represented by the vector $x_c = [I_c(1), I_c(2), L, I_c(z \times p \times z \times p)]$, where $I_c(v)$ is an indicator number showing whether a fine spatial resolution pixel v belongs to the class c, and is defined as:

$$I_c(v) = \begin{cases} 1 & \text{if fine spatial resolution pixel } v \text{ labelled with the land cover class } c \\ 0 & \text{otherwise} \end{cases} \tag{2}$$

Thus, x_c represents the spatial distribution of fine spatial resolution pixels of the class c.

A patch pair of the class 1

	0	1/4	0
	1/4	1	3/8
	0	3/8	3/16

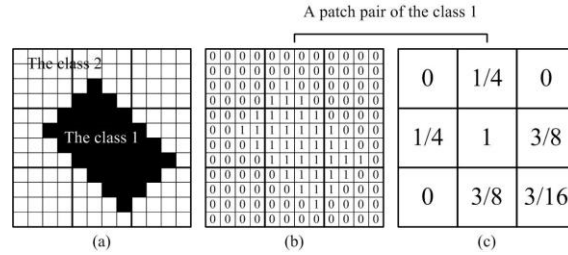(a)   (b)   (c)

Fig. 1. A patch pair example, where the zoom factor is 4 and the coarse spatial resolution patch size is 3. (a) is a fine spatial resolution land cover map including 12×12 pixels of two land cover classes, 1 (black) and 2 (white); (b) is the corresponding fine resolution patch of the class 1, where the number 1 indicates that the fine resolution pixel belongs to the class 1, and 0 indicates that the fine resolution pixel belongs to other classes; (c) is the corresponding coarse resolution patch, where the number within pixels is the area percentages of the class 1 in each coarse spatial resolution pixel.

Fig. 1 shows a patch pair example with $p = 3$ and $z = 4$. Fig. 1(a) is a fine spatial resolution land cover map including two classes. For the land cover class 1, as shown in black in Fig. 1(a), the fine and coarse spatial resolution land cover patches are shown in Fig. 1(b) and Fig. 1(c), respectively. The fine spatial resolution patch is an indicator map [Fig. 1(b)], where a label 1 means that the fine pixel belongs to the class 1, and 0 means that the fine spatial resolution pixel belongs to other classes. Therefore, the indicator map

$$x_1 = [\underbrace{0,0,...,0}_{\text{The first line}},...,\underbrace{1,1,1,1,1,1,1,1,1,0,0,0}_{\text{The 5th line}},...,\underbrace{0,0,...,0}_{\text{The 12th line}}]$$ shows the spatial pattern of the class 1. The coarse patch is the fraction image of the class, where the value represents the area percentages within each coarse pixel, and is

represented as $y_1 = [0, \frac{1}{4}, 0, \frac{1}{4}, 1, \frac{3}{8}, 0, \frac{3}{8}, \frac{3}{16}]$. Together $[x_1, y_1]$ is a patch pair for the class 1.

Once a large number of patch pairs available, the SRM problem can then be solved by using a pattern matching method. Given a coarse spatial resolution patch in the input fraction images, the patch pairs that have similar coarse spatial resolution patches are selected from those available patch pairs. These selected patch pairs are called as neighboring patch pairs, because if all patch pairs are listed in order according to the fraction values, they are located in neighboring sites. It is noted that these neighboring patch pairs all include a coarse spatial resolution patch and a fine spatial resolution patch. Because coarse spatial resolution patches with similar

fraction values often have similar spatial land cover patterns, the latent fine spatial resolution patch for the coarse spatial resolution patch in the input fraction images should be similar with the fine spatial resolution patch included in the neighboring patch pairs. Thus, the SRM seeks to make the spatial land cover pattern of the resultant fine spatial resolution land cover map match those of neighboring patch pairs.

In general, in the proposed learning based SRM algorithm, the fine and coarse spatial resolution patch pairs are first extracted from available fine spatial resolution land cover maps to produce a learning database. Similar patch pairs are then found for each coarse spatial resolution patch in input fraction images. Finally, these available patch pairs in the learning database are used to reconstruct the final fine spatial resolution land cover map. All these steps are described in detail as follows.

C. Generating the training database

Finding the relationship between the fine spatial resolution land cover maps and coarse spatial resolution fraction images, which is represented by patch pairs in the training database, is one of the key issues of the proposed learning based SRM algorithm. Here, the patch pairs are generated class by class. Given a set of fine spatial resolution land cover maps, a corresponding set of coarse spatial resolution patches for each land cover class can be produced from them.

An example fine spatial resolution land cover map which includes three land cover classes, as shown in Fig. 2(a), is used to illustrate the training database generation procedure. Before the training database is generated, the zoom factor z and the coarse spatial resolution patch size p are set. In this example, z is set to be 4, and p is set to be 3. A fine spatial resolution patch then includes $z \times p \times z \times p$ fine spatial resolution pixels (equals to 12×12 in this example). In order to generate a patch pair, a fine spatial resolution land cover map with the size of $z \times p \times z \times p$ is first exacted. Generally, by moving a fixed window containing $z \times p \times z \times p$ rows and columns within the original land cover map, various fine spatial resolution maps can be extracted.

These extracted fine spatial resolution maps can be overlapped, thus the fine spatial resolution land cover pattern included in the original land cover map is fully exploited. For an extracted fine spatial resolution map, as shown in Fig. 2(b), one fine spatial resolution patch, that is, one indicator map was then generated for each land cover class, as shown in Fig. 2(c)-(e). For each fine spatial resolution patch, the corresponding coarse spatial resolution patch consists of fraction values of all coarse spatial resolution pixels. Each coarse spatial resolution pixel corresponds to $z \times z$ fine spatial resolution pixels, and the fraction value $f_c(V)$, which is the percentage of the fine spatial resolution pixels assigned to the class c in the coarse spatial resolution pixel V, is calculated as:

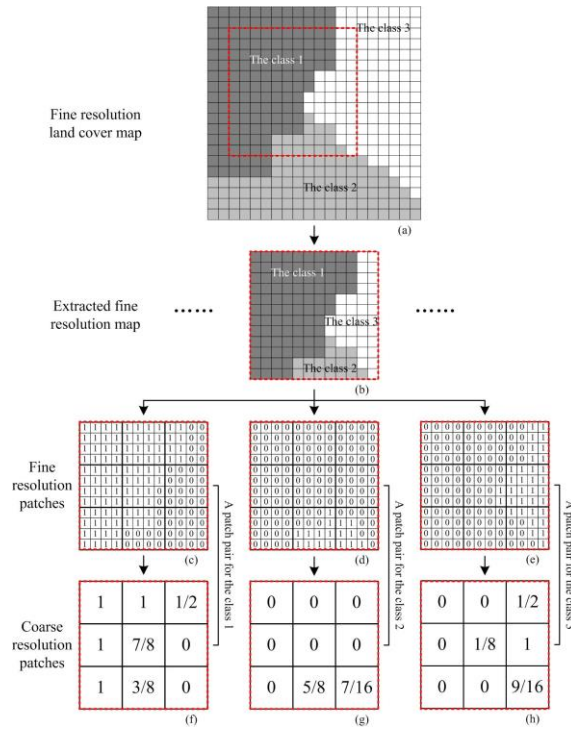$$f_c(V) = \sum_{v \in V} I_c(v) \Big/ z^2 \tag{3}$$

Fig. 2. An example of the training database generation procedure, where the zoom factor is 4 and the coarse resolution patch size is 3. (a) is the original fine resolution land cover map; (b) is one fine resolution land cover map including 12×12 fine resolution pixels extracted from the original fine resolution land cover map. (c), (d) and (e) are fine resolution patches of different land cover classes, which are generated from the extracted fine resolution land cover map. The number 1 indicates that the fine resolution pixel belongs to the class, and 0 indicates that the fine resolution pixel belongs to other classes; (f), (g) and (h) are corresponding coarse resolution patches generated from (c), (d) and (e), where the number within pixels means the area percentages of different class in each coarse resolution pixel. One fine resolution patch and one coarse resolution patch form a patch pair, including (c) and (f), (d) and (g), and (e) and (h) for three different land cover classes.

Each extracted fine spatial resolution map (Fig. 2) can generate one patch pair for each land cover class. Supposed that K different fine spatial resolution maps are extracted from the original fine spatial resolution land cover map, K patch pairs can be generated for each class. Those patch pairs comprise the training database, where the fine spatial resolution patches are represented as $X_{T,c} = \{x_{T,c}^i\}_{i=1}^K$ and the coarse spatial resolution patches are represented as $Y_{T,c} = \{y_{T,c}^i\}_{i=1}^K$ for class c.

D. Searching neighboring patch pairs

Once the training database has been built, it is used to provide land cover information to estimate the latent fine spatial resolution land cover map with input coarse spatial resolution fraction images. For each coarse spatial resolution patch in the input fraction images, neighboring training patch pairs that have similar coarse spatial resolution patch are searched from the training database. Since the training database is generated class by class, the search procedure is also performed class by class. Let $Y_{F,c} = \{y_{F,c}^i\}_{i=1}^R$ be coarse spatial resolution patches in the input fraction images F for class c. For the ith coarse spatial resolution patch $y_{F,c}^i$, its neighboring training patch pairs are chosen according to the following criterion:

$$\Delta f(y_{F,c}^i, y_{T,c}^{i,j}) = \sqrt{\frac{1}{p \times p} \sum (f_{F,c}^i(V) - f_{T,c}^{i,j}(V))^2} < T_L \tag{4}$$

where $\Delta f(y_{F,c}^i, y_{T,c}^{i,j})$ is the difference of fraction values between coarse spatial resolution patch $y_{F,c}^i$ in the fraction image and the jth corresponding patch $y_{T,c}^{i,j}$ in the training database. $f_{F,c}^i(V)$ is the fraction value of the class c of the coarse spatial resolution pixel V in $y_{F,c}^i$, and $f_{T,c}^{i,j}(V)$ is the fraction value of the class c of the corresponding coarse spatial resolution pixel V in $y_{T,c}^{i,j}$. The more similar the coarse spatial resolution patches are, the lower the value of Δf. The threshold T_L is the tolerable fraction difference between two patches. If the value of $\Delta f(y_{F,c}^i, y_{T,c}^{i,j})$ is no more than that of T_L, $y_{T,c}^{i,j}$ is thus considered the similar patch of $y_{F,c}^i$, and the patch pair that includes $y_{T,c}^{i,j}$ is the neighboring training patch pair. The value of T_L is an

important parameter for searching neighboring patch pairs. If it is too large, the neighboring patch pairs are too different with that of the input fraction images to provide accurate land cover information. On contrast, if T_L is too small, only few neighboring patch pairs can be found, leading to insufficient land cover information. The effect of the value of T_L will be assessed in our later experiments.

The k-dimensional (K-D) tree algorithm is applied to find neighboring training patch pairs in the present work, due to its efficient and successful application in the image super-resolution field [57]. The K-D tree organizes coarse spatial resolution patches in the training database off-line to enable a fast search by defining a binary tree of thresholds, which are chosen optimally so as to expedite the search. Moreover, the K-D tree relies on a special high dimensional data structure and thus the neighbors searching step can be speeded up significantly. More detailed information about the K-D tree can be found in references [57, 58].

For each coarse spatial resolution patch in the input fraction images F, the neighboring coarse spatial resolution patches and their corresponding fine spatial resolution patches are searched from the training database using the K-D tree algorithm. A simple example for a two class situation given in Fig. 3 is used to illustrate the neighboring training patch pairs searching procedure. In this example, the coarse spatial resolution patch size p is set to be 3, and one coarse spatial resolution patch then includes 3×3 coarse spatial resolution pixels. For a coarse spatial resolution pixel in the fraction image, all nine coarse spatial resolution patches that include this coarse spatial resolution pixel are extracted, by scanning the entire fraction images F. For each coarse spatial resolution patch $y_{F,c}^i$, we search the neighboring coarse spatial resolution patches from the training database. The neighboring training patch pairs $\{x_{T,c}^{i,j}, y_{T,c}^{i,j}\}_{j=1}^{k_i}$, where k_i is the number of the searched patches, are then used to estimate the latent fine spatial resolution land cover map, as described below.
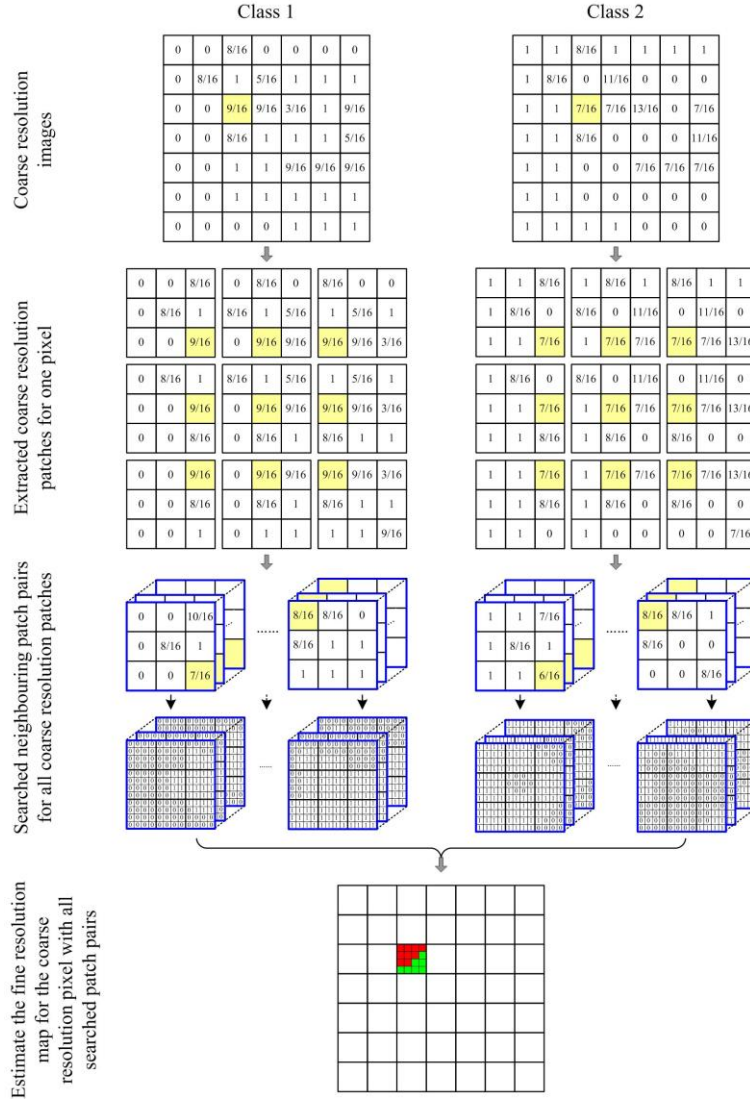
Fig. 3. An example of the fine resolution land cover map estimation procedure, where the coarse resolution patch size is 3. Two land cover classes are included. For one pixel, all relative coarse resolution patches are extracted for the input fraction images for each class. The neighboring patch pairs are selected from the training database for each exacted coarse resolution patch. All selected patch pairs are then used to estimate the resultant fine resolution land cover map, which shows the distribution of the classes and is still in correct proportion in the input fraction images (9/16 and 7/16, respectively).

E. Estimating the fine spatial resolution land cover map

The fundamental assumption of the proposed learning based SRM algorithm is that coarse spatial resolution patches with similar class fraction values have similar fine spatial resolution land cover patterns. In order to estimate the latent fine spatial resolution land cover map, the proposed SRM algorithm aims to make the fine spatial resolution patches in the latent fine spatial resolution land cover map similar with the fine spatial

resolution patches identified from the selected neighboring training patch pairs. Therefore, the objective of the SRM is to obtain a minimal difference between the fine spatial resolution patch in the estimated fine spatial resolution land cover map and corresponding fine spatial resolution patches in the neighboring training patch pairs. During the estimation process, all coarse spatial resolution pixels in the input fraction images are handled simultaneously, and SRM can be addressed by using the following minimization optimization model:

$$Min \quad \varepsilon(\hat{H}^L) = \sum_{c=1}^{C}\sum_{i=1}^{M\times N}\sum_{j=1}^{k_i} w_L(x_{T,c}^{i,j}) \bullet E(x_{T,c}^{i,j}, x_{\hat{H},c}^i) \tag{5}$$

$$E(x_{T,c}^{i,j}, x_{\hat{H},c}^i) = \sqrt{\frac{1}{z\times p\times z\times p}\sum_{v=1}^{z\times p\times z\times p}(I_{T,c}^{i,j}(v)-I_{\hat{H},c}^i(v))^2} \tag{6}$$

$$w_L(x_{T,c}^{i,j}) = 1-\Delta f(y_{T,c}^{i,j}, y_{\hat{H},c}^i) = 1-\Delta f(y_{T,c}^{i,j}, y_{F,c}^i) \tag{7}$$

Subject to

$$\sum_{c=1}^{C} I_{\hat{H},c}(v) = 1, \tag{8}$$

$$\sum_{v\in V} I_{\hat{H},c}(v) = f_{\hat{H},c}(V)\times z^2 \quad \text{for all } V\in F. \tag{9}$$

where $\hat{H}^L$ is the fine spatial resolution land cover map that we aim to estimate. Setting the coarse spatial resolution patch size to be odd without loss of generality, $y_{F,c}^i$ is the coarse spatial resolution patch in which the ith coarse spatial resolution pixel is located in the patch center in the fraction images F. Note that $y_{F,c}^i$ is the same as $y_{\hat{H},c}^i$ because the values in F are preserved in $\hat{H}^L$ as (1). $x_{\hat{H},c}^i$ is the corresponding fine spatial resolution patch of $y_{\hat{H},c}^i$ in $\hat{H}^L$ for the class c. $\{x_{T,c}^{i,j}\}_{j=1}^{k_i}$ are fine spatial resolution patches corresponding to the coarse spatial resolution patches $\{y_{T,c}^{i,j}\}_{j=1}^{k_i}$ in the selected neighboring training patch pairs. $E(x_{T,c}^{i,j}, x_{\hat{H},c}^i)$ is the difference between two fine spatial resolution patches, $x_{\hat{H},c}^i$ and $x_{T,c}^{i,j}$, and is computed as (6), where $I_{\hat{H},c}^i(v)$ is the indictor of the fine spatial resolution pixel v within $x_{\hat{H},c}^i$, and $I_{T,c}^{i,j}(v)$ is the indicator of the fine spatial resolution pixel v within $x_{T,c}^{i,j}$, respectively. $w_L(x_{T,c}^{i,j})$ is the weight value assigned to the fine spatial resolution patch $x_{T,c}^{i,j}$, and is computed in the coarse spatial resolution scale by comparing the fraction difference between two corresponding coarse spatial resolution patches as (7). The larger the fraction difference, lower the

weight value. Moreover, Equation (8) ensures that each fine spatial resolution pixel is assigned one and only one land cover class, and Equation (9) is the area constraint provided by the input coarse spatial resolution fractions for all coarse spatial resolution pixels.

The minimization problem has a large solution space, which increases with the number of neighboring fine spatial resolution patches, land cover classes, and the image size. To solve the problem within a short computational time, this work used a simulated annealing algorithm to find the solution. A power-law annealing schedule is used in the simulated annealing algorithm [59], where the temperature Tem_n at iteration n is modified according to

$$Tem_n = \sigma \cdot Tem_{n-1} \tag{10}$$

where $\sigma \in (0,1)$ controls the decrease rate of temperature Tem_n.

In the initialization step, the fine spatial resolution pixels of each class within each coarse spatial resolution pixel are randomly labeled according to the input coarse spatial resolution fractions. In this situation, the constraints in (8) and (9) are naturally satisfied. In each iteration, two fine spatial resolution pixels with different land cover labels are randomly selected in each coarse spatial resolution pixel. The values are then calculated by using equation (5) according to the current fine spatial resolution land cover map configuration. If swapping these two fine spatial resolution pixels decreases the object function value in equation (5), these two fine spatial resolution pixels are swapped. Otherwise, the swap can only be accepted with a small probability according to the current temperature in equation (10). The algorithm stops when the previously fixed number of iterations is achieved.

F. Patch outlier rejection

The above-proposed minimization optimization model should be generally considered as a simple fine spatial resolution pixel averaging method. This model has limitations, notably that the derived fine spatial

resolution map may be disrupted because of the problem of patch outliers. In general, a fine spatial resolution

patch only corresponds to one coarse spatial resolution patch, and their relationship is shown in equation (3). But

on the contrary, given a coarse spatial resolution patch, many different fine spatial resolution patches can

correspond to it, making SRM be an underestimated inversion problem [28].
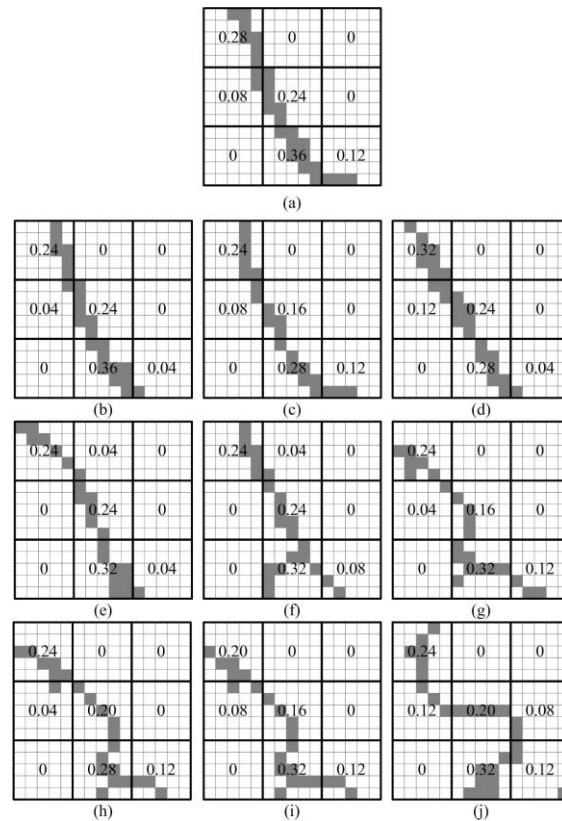

Fig. 4. An example of patch outliers in selected neighboring patch pairs. (a) is a patch pair for one land cover class. The fine resolution patch includes 15×15 pixels and the coarse resolution patch includes 3×3 pixels. The fine resolution pixel filled by grey color indicates that it belongs to the class. The number within pixels means the area percentages of class in each coarse resolution pixel of the class. (b) to (j) are searched neighboring patch pairs of (a) using the tolerable fraction difference value. The fraction values in (b) to (j) are similar with the fraction values in (a), however, only fine spatial resolution patches in (b) and (c) are similar with that in (a). Fine spatial resolution patches in (g)-(j) are much different with that in (a).

Fig. 4 presents an example of a patch outlier. In Fig. 4(a), a patch pair is taken from an experiment reported

below. This patch pair includes a coarse spatial resolution patch of size 3×3, and a fine spatial resolution patch

of size 15×15. The numbers within coarse spatial resolution pixels mean the fraction values of the class. Grey

fine spatial resolution pixels represent the pixels belonging to this class, and white fine spatial resolution pixels

represent the pixels belonging to other classes. Searching in a training database including 120,000 patch pairs by using the coarse spatial resolution patch in Fig. 4(a) as the reference, the resultant 9 neighboring patch pairs are simultaneously shown in Figs. 4(b)-(j). As the neighboring patch pairs are searched by comparing the fraction different between coarse spatial resolution patches, coarse spatial resolution patches in these neighboring patch pairs are all much similar to the coarse spatial resolution patch in the reference patch pair. When comparing the fine spatial resolution patches, it is noticed that only fine spatial resolution patches in Fig. 4(b) and Fig. 4 (c) are very similar with those in Fig. 4(a). Fine spatial resolution patches in Figs. 4(g)-(j) are very different with those in Fig. 4(a), and are then not suitable to be applied to estimate the fine spatial resolution patch. Therefore, in order to improve the performance of the learning based SRM algorithm, only the patch pairs which have similar fine spatial resolution patches with the reference should be applied to estimate the latent fine spatial resolution land cover map, and other patch pairs should be considered as outliers.

For the fine resolution patch $x_{T,c}^{i,j}$ within the neighboring training patch pairs, it is defined as the outlier patch according to the following criterion:

$$\Delta f(x_{T,c}^{i,j}, x_{H,c}^{i}) = \sqrt{\frac{1}{z \times p \times z \times p} \sum_{v=1}^{z \times p \times z \times p} (I_{T,c}^{i,j}(v) - I_{H,c}^{i}(v))^2} \geq T_h \tag{11}$$

where $\Delta f(x_{T,c}^{i,j}, x_{H,c}^{i})$ is the difference between two fine spatial resolution patches, and is computed as same as $E(x_{T,c}^{i,j}, x_{H,c}^{i})$ is equation (6). $x_{H,c}^{i}$ is the fine spatial resolution patch in the latent fine spatial resolution land cover map, and $x_{T,c}^{i,j}$ is the fine resolution patch within the neighboring training patch pairs. The more similar the fine resolution patches are, the lower the value of $\Delta f(x_{T,c}^{i,j}, x_{H,c}^{i})$. The threshold T_h is the tolerable difference between two fine spatial resolution patches. If the value of $\Delta f(x_{T,c}^{i,j}, x_{H,c}^{i})$ is no less than that of T_h, the fine spatial resolution patch $x_{T,c}^{i,j}$ is considered as an outlier patch.

In the object function (5), $w_L(x_{T,c}^{i,j})$ is used to give the weight values. However, this weight value is computed by comparing coarse spatial resolution patches and is then not sufficient to distinguish outliers from

the selected neighboring patch pairs. In order to consider the outlier patches, an additional patch weight

$w_H(x_{T,c}^{i,j})$ that is computed at the fine spatial resolution is added in the object function of the proposed SRM

algorithm as:

$$Min \quad \varepsilon(\mathbf{H}) = \sum_{c=1}^{C} \sum_{i=1}^{M \times N} \sum_{j=1}^{k_i} w_L(x_{T,c}^{i,j}) \bullet w_H(x_{T,c}^{i,j}) \bullet E(x_{T,c}^{i,j}, x_{H,c}^{i}) \tag{12}$$

$$w_H(x_{T,c}^{i,j}) = \begin{cases} 0 & \text{If } \Delta f(x_{T,c}^{i,j}, x_{H,c}^{i}) \geq T_h, \text{ the patch is an outlier} \\ 1 & \text{Otherwise, the patch is not an outlier} \end{cases} \tag{13}$$

In general, if the patch $x_{T,c}^{i,j}$ is an outlier, the weight value $w_H(x_{T,c}^{i,j})$ is set to be zero, meaning that this

fine spatial resolution patch no longer used during the estimation procedure. Otherwise, the weight value

$w_H(x_{T,c}^{i,j})$ is set to be one, if the patch is not the outlier.
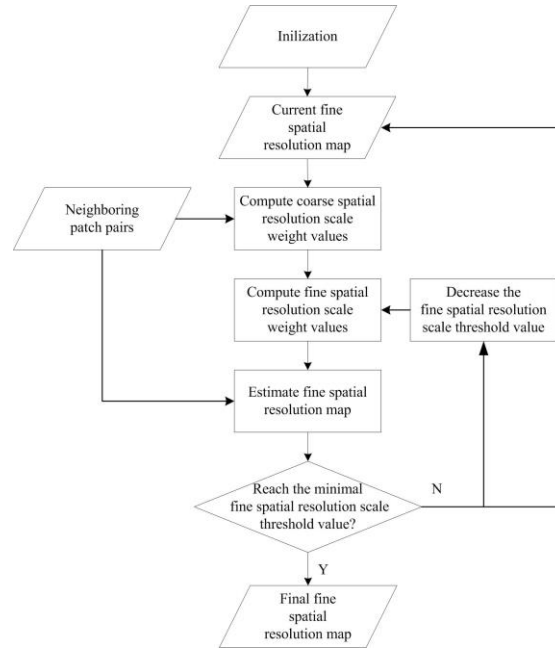

Fig. 5. The flowchart of the iterative patch outlier handling procedure.

Setting an appropriate value of T_h is important if patch outliers are to be addressed effectively. In the

present work, an iterative method is used. The main iteration procedure is shown in Figure 5. At first, a fine

spatial resolution land cover map is estimated according to the minimization optimization model (5), using all

searched neighboring learning patch pairs. Because all neighboring patch pairs are searched by using a tolerant

fraction value T_L as (4), it is expected that the estimated fine spatial resolution land cover map is similar with

the latent fine spatial resolution land cover map. Then, we begin to refine the estimated fine spatial resolution land cover map, by decreasing the value of T_h step by step, from the maximal threshold T_h^{Max} to the minimal threshold T_h^{Min}. With each value of T_h, a new fine spatial resolution land cover map is estimated according to (12). At the beginning, with a large T_h value, only a relatively small amount of neighboring patches, whose fine spatial resolution patches are markedly different to the current estimated fine spatial resolution land cover map, are considered as outlier. Without these patch outliers, a more accurate fine spatial resolution land cover map is expected to be estimated. The value of T_h decreases iteratively and more patches are considered as outliers. Then, the estimated fine spatial resolution land cover map is expected to be more accurate. At the end, the iteration converges to a stable solution until the minimal value T_h^{Min} is reached, and the estimated fine spatial resolution land cover map is considered as the result of SRM.

G. The proposed algorithm

According to the aforementioned principles, we summarize the proposed learning based SRM algorithm in Algorithm 1. In brief, a fine spatial resolution land cover map is first randomly generated using input coarse spatial resolution fraction images in the initialization step. Meanwhile, the patch pairs in the training database are constructed according to the zoom factor and the coarse spatial resolution patch size. The input coarse spatial resolution fraction images are then scanned and neighboring patch pairs are searched by the K-D tree algorithm, for all coarse spatial resolution patches in fraction images class by class. Using these searched neighboring patch pairs, the initial fine spatial resolution land cover map is estimated by using the simulated annealing algorithm. Outliers in these neighboring patch pairs are then found and the fine spatial resolution land cover map is re-estimated, by changing the threshold value T_h. Once T_h reaches T_h^{Min}, the iteration is finished, the estimated fine spatial resolution land cover map is the result of the learning based SRM algorithm.

<div align="center">Algorithm I</div>

Objective: Estimate fine spatial resolution land cover map H

Input: Coarse spatial resolution fraction images F, zoom factor z, land cover class number C, coarse spatial resolution patch size p, coarse spatial resolution fraction threshold T_L, the maximal and minimal fine spatial resolution thresholds T_h^{Max} and T_h^{Min}, fine spatial resolution threshold change value dT_h, parameters of the simulated annealing algorithm: Tem_0, σ, and Ite.

1. Initialization:

1) For each coarse spatial resolution pixel, calculate the number of fine spatial resolution pixels for each class as (1);

2) Randomly set class label for all fine spatial resolution pixels using the number as the constraints;

2. Training database generation

1) Extract fine spatial resolution patches from available land cover maps;

2) Estimate the corresponding coarse spatial resolution patch for each fine spatial resolution patch and generate patch pairs in the training database;

3. Similar Patch Finding

1) Build the K-D tree for all coarse spatial resolution patches in the training database;

2) Scan F, and extract all coarse spatial resolution patches;

3) Search neighboring patch pairs from the training database for all coarse spatial resolution patches in F.

4. Generating initial high resolution land cover map

1) Reconstruct H^L by minimizing the objective function in (5) using the simulated annealing algorithm.

5. Iterative patch outlier rejection

1) Set $T_h = T_h^{Max}$

2) Do {

[1] Calculate the weight values using current H^L and T_h, according to (13);

[2] Reconstruct H^L according to (12);

[3] $T_h = T_h - dT_h$;

} Until $T_h \leq T_h^{Min}$

Result: Output the fine spatial resolution land cover map H^L.

III. EXAMPLE

The National Land Cover Database 2001 (NLCD 2001) that shows the land cover for the conterminous

USA was used to test the proposed learning based SRM algorithm. NLCD 2001 is a raster-based 16-class land

cover map over all 50 US states and Puerto Rico at spatial resolution of 30 m, and is primarily generated from the unsupervised classification of Landsat Enhanced Thematic Mapper Plus circa 2001 satellite dataset [60]. To simplify the experiment, the original 16 classes of the NLCD images were converted into simple class scheme which includes four general land cover classes: water, urban, forest and agriculture.
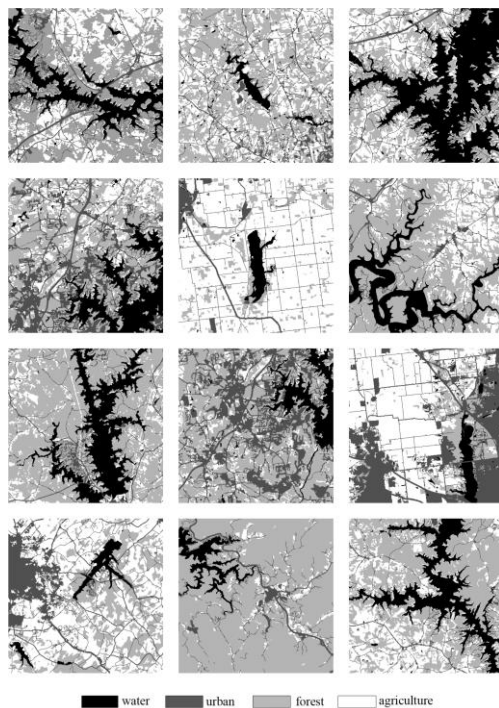

Fig. 6. All 12 subsets of NLCD land cover maps used to generate the training database. Each subset has 400×400 pixels and four land cover classes.
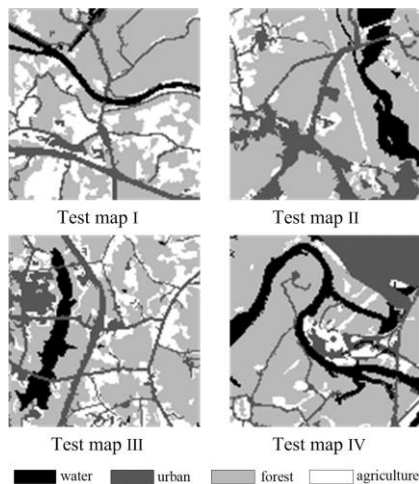

Fig. 7. Four subset NLCD land cover maps (with 120×120 pixels) used to test the proposed algorithm.

We select twelve subsets of NLCD maps (each contains 400×400 pixels) as shown in Fig. 6 to generate the coarse and fine spatial resolution patch pairs, which formed the training database. A further four subsets of NLCD maps (each contains 120×120 pixels; Fig.7), were used to assess the proposed SRM algorithm. These twelve subsets are called as training maps and the four subsets are called as test maps. The locations of these four test maps are different to those of the twelve training maps used to construct the training database. For each of the four test maps, we generate synthetic coarse fraction images by linear averaging the fine spatial resolution pixel number within the coarse spatial resolution pixel according to different zoom factors. Using simulated fraction images as input, as well as the constructed training database, the proposed SRM algorithm is applied to estimate a fine spatial resolution land cover map. In order to assess the accuracy of the proposed learning based SRM algorithm, by using the test land cover maps as the reference, the overall accuracy (OA) and Kappa coefficient are used to evaluate the accuracy of the estimated land cover maps, by comparing the entire estimated map with the corresponding reference map.

The proposed learning based SRM algorithm was also compared with the pixel-based hard classification method (HC) and several popular SRM algorithms including the pixel swapping algorithm based on simulated annealing (PS) [61], the sub-pixel/pixel attraction algorithm (SPA) [29], the bilinear interpolation based algorithm (BI) [56] and the BP neural network based algorithm (BP) [53]. It is noted that the input of PS, SPA and BI algorithms includes only coarse spatial resolution fraction images, because all these SRM algorithms describe the land cover distribution using the spatial dependence principle. By contrast, the input of BP algorithm includes not only the coarse spatial resolution fraction images, but also fine spatial resolution land cover maps that are used to learn prior land cover information. In the experiments, all twelve training maps are used in the BP algorithm.
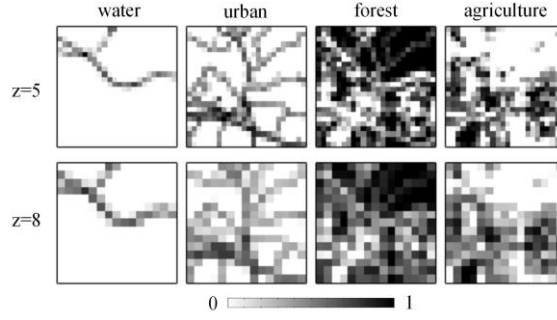
Fig. 8. Simulated fraction image generated from the test map I as shown in Fig. 7. The top row presents the fraction images at $z = 5$, and the bottom row presents the fraction images at $z = 8$.

The test map I as shown in Fig. 7(a), was first used to assess the impact of parameters in the proposed SRM algorithm. Synthetic fraction images, as shown in Fig. 8, were simulated from the fine spatial resolution test map I. Two zoom factors, $z = 5$ and $z = 8$, were applied. The fine and coarse spatial resolution patch pairs in the training database were generated from all twelve training maps as shown in Fig. 6 with zoom factors of 5 and 8, respectively.

When the proposed learning based SRM algorithm is performed, the resultant fine spatial resolution land cover map is affected by parameters used in the algorithm. According to our experiments, the coarse patch size p was set to be 3, because a large p value makes the spatial structure of a coarse patch too complex to find enough similar image patches. T_h^{Max} was set to 1, meaning that no fine spatial resolution neighboring patches are considered as outliers at the beginning. dT_h was set to 0.05, in order to decrease the value of T_h gradually. Moreover, to further assess the impact of parameter values on the performance of the proposed method, three most important parameters including the number of patch pairs in the training database, the coarse spatial resolution fraction difference threshold value T_L and the minimal fine spatial resolution difference threshold value T_h^{Min} are discussed in the following sections, respectively.
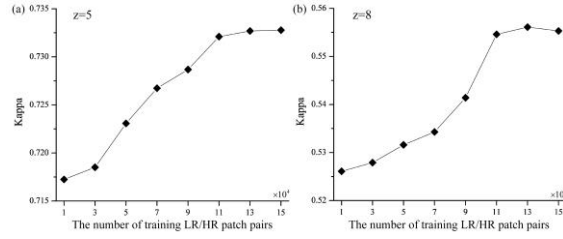
Fig. 9. Kappa values of the resultant fine resolution land cover maps of the proposed learning based SRM algorithm with different numbers of training patch pairs. (a) is the result at $z = 5$; (b) is the result at $z = 8$.

1) Impact of the number of patch pairs in the training database: To assess the impact of the number of patch pairs in the training database, the analysis was repeated 8 times over the range of $[1 \times 10^4, 15 \times 10^4]$ with an interval of 2×10^4. Fig. 9 indicates the Kappa values of resultant fine spatial resolution land cover maps produced by the learning based SRM algorithm with different numbers of patch pairs in the training database, at zoom factors of 5 and 8, respectively. When the number is less than 3×10^4, the Kappa values of the results at $z = 5$ and $z = 8$ are both at a low level. This is because the use of only a few patch pairs cannot provide enough information about the spatial land cover patterns. With the increment of the number, both Kappa values at $z = 5$ and $z = 8$ increase rapidly until the number reaches to about 11×10^4, and then the Kappa values maintain stable, as shown in Figs. 9 (a) and (b). It is also noticed that the increment of Kappa values at $z = 5$ is more rapid than that at $z = 8$, when the number is in the range of $[3 \times 10^4, 9 \times 10^4]$. The reason is that more patch pairs are needed in order to decrease the uncertainty caused by a large zoom factor. According to the experiment, a number of patch pairs larger than 11×10^4 is reasonable. As more patch pairs may increase the calculation burden, the number of patch pairs in the training database is set to be 12×10^4 in our latter experiments.

2) Impact of the threshold T_L: The threshold value T_L is a pre-defined parameter that represents the tolerable fraction difference between two coarse spatial resolution patches. This parameter guarantees that the searched coarse spatial resolution patch which has a fraction difference Δf larger than T_L cannot be accepted as the candidate image patch. Fig. 10 shows the Kappa values of the resultant fine spatial resolution land cover

maps produced by the proposed learning-based SRM algorithm with different T_L values. When T_L is in the range of $[0.02, 0.14]$ at $z = 5$ and in the range of $[0.02, 0.12]$ at $z = 8$, the Kappa values increase with the increment of the value of T_L. This is because that the number of candidate patch pairs is too small to provide enough land cover pattern information for SRM, if T_L is set to be a too low value. For $z = 5$, as shown in Fig. 10(a), if the value of T_L is larger than 0.14, the Kappa values are kept at a stable level. For $z = 8$, however, the Kappa values begin to decrease until a stable value, if T_L is larger than 0.12. In general, with a larger value of T_L, more patch pairs with larger fraction errors are considered as candidate patches, which indeed generally provide erroneous information and make the estimated fine spatial resolution land cover map differ significantly from the latent map. Setting too large a value of T_L may degrade the estimated fine spatial resolution map. However, the result is only slightly different because of the additional patch outlier rejection procedure.
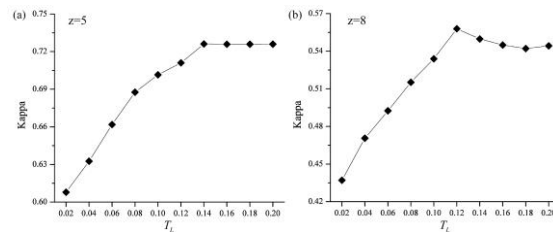

Fig. 10. Kappa values of the resultant fine resolution land cover maps of the proposed learning based SRM algorithm with different values of coarse resolution threshold T_F. (a) is the result at $z = 5$; (b) is the result at $z = 8$.

Fig. 11. Kappa values of the resultant fine resolution land cover maps of the proposed learning based SRM algorithm with different minimal fine resolution threshold T_h^{Min}. (a) is the result at $z = 5$; (b) is the result at $z = 8$.
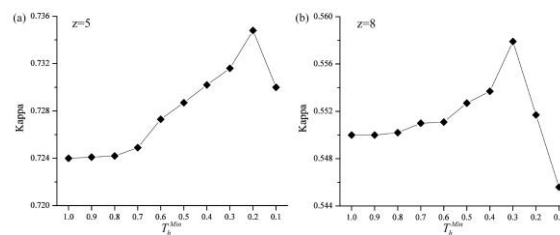
3) Impact of the minimal fine spatial resolution threshold of T_h^{Min}: The value of T_h^{Min} is denoted as the minimal threshold value, which is used to distinguish the outlier patches from all neighboring patches in the

estimation procedure. To assess the impact of the T_h^{Min} value, the learning based SRM algorithm was applied

with different values of T_h^{Min} in the range of $[1.0, 0.1]$ with an interval of -0.1. The Kappa values of the

resultant fine spatial resolution land cover maps produced by the proposed learning based SRM algorithm at

$z = 5$ and $z = 8$ are shown in Fig. 11. With the decrement of the values of T_h^{Min}, the corresponding Kappa

values of the resultant fine spatial resolution land cover maps increase, because more coarse spatial resolution

patches are considered as outlier patches and not used in the estimation procedure. When T_h^{Min} is larger than 0.2

at $z = 5$ and 0.3 at $z = 8$, however, the Kappa values begin to decrease as the value of T_h decreases. The

reason is that most neighboring patches are considered as outliers if the value of T_h is too low, and the

remaining neighboring patches can not provide enough information for SRM.
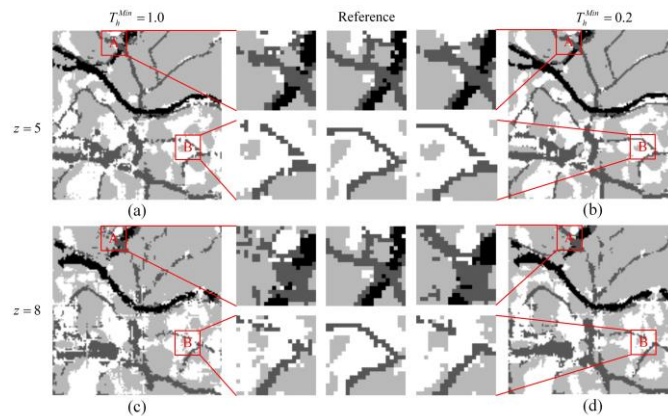

Fig. 12. Resultant fine resolution land cover maps produced by the proposed learning based SRM algorithm. (a) is the result without

patch outlier handling procedure and (b) is the result using patch outlier handling procedure at $z = 5$. (c) is the result without

patch outlier handling procedure and (d) is the result using patch outlier handling procedure at $z = 8$. Using the patch outlier

handling procedure reduces the salt-and-pepper artifacts as shown in the enlarged part A, and the linear discontinuities as shown in

the enlarged part B.

A visual comparison, as shown in Fig. 12, is used to further assess the impact of the value of T_h^{Min}. For

$z = 5$, as shown in Fig. 12(a), many salt-and-pepper artifacts appear and the spatial continuities of some linear

features are interrupted when $T_h^{Min} = 1.0$, which means that all patches are accepted and no outliers exist. In

contrast, with patch outlier rejection (when $T_h^{Min} = 0.2$), most of the salt-and-pepper artifacts are eliminated and

the spatial continuities are well maintained, as shown in Fig. 12(b). The impact of T_h^{Min} on the resultant fine spatial resolution land cover map is more obvious when $z = 8$. Many salt-and-pepper artifacts and linear discontinuities that appear in the fine spatial resolution land cover map, as shown in Fig. 12(c), are eliminated by the outlier rejection, as shown in Fig. 12(d).
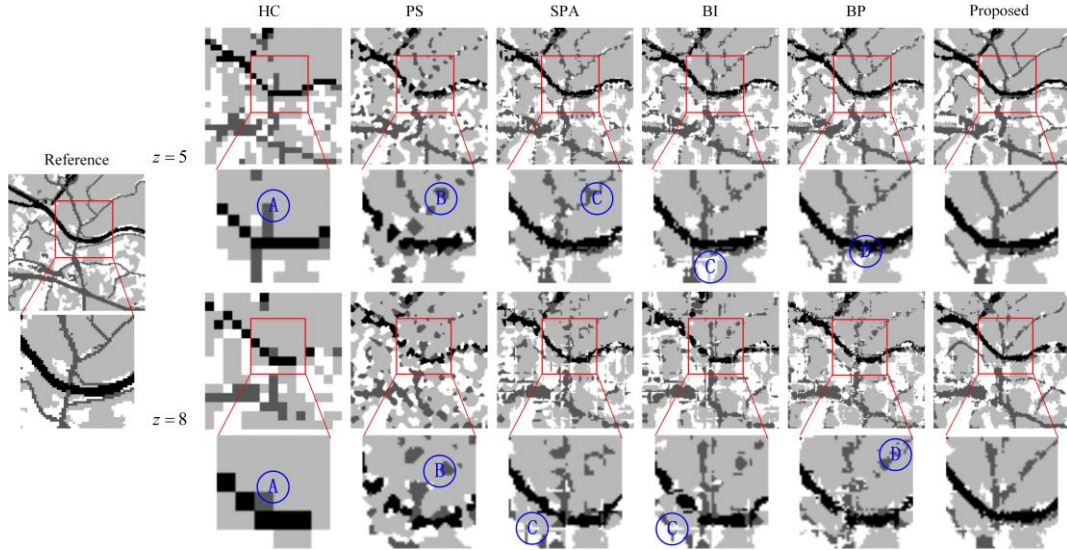

Fig. 13. Resultant land cover maps generated by different methods with $z = 5$ and $z = 8$ for the test map I. HC produces jagged boundaries (such as the area A); PS produces isolated patches (such as the area B); SPA and BI produce linear artifacts (such as the area C); and BP produces salt-and-pepper artifacts and isolated patches (such as the area D).

4) Comparison with other methods: According to aforementioned discussion about parameters used in the proposed learning based SRM method, the optimal parameter values were used to produce the resultant fine spatial resolution land cover maps. In particular, the number of patch pairs in the learning database is 12×10^4, the value of T_f is 0.12, and the value of T_h^{Min} is 0.2 for $z = 5$ and 0.3 for $z = 8$, respectively. By using the same aforementioned simulated coarse fraction images used for the proposed learning based SRM method as input, the resultant land cover maps of HC, PS, SPA, BI, BP and the proposed learning based SRM are all shown in Fig. 13. Additionally, the Kappa and OA values of all these maps produced by different methods are shown in Table. I.

Table I. Kappa and Overall Accuracy (OA) values of the resultant land cover maps produced by different methods at $z=5$ and $z=8$ for the test map I.

		HC	PS	SPA	BI	BP	Proposed
z=5	Kappa	0.6223	0.6525	0.6780	0.6856	0.7050	0.7348
	OA	0.7735	0.7890	0.8045	0.8091	0.8209	0.8390
z=8	Kappa	0.4811	0.4739	0.5068	0.5148	0.5264	0.5561
	OA	0.6957	0.6806	0.7006	0.7054	0.7124	0.7305

In general, for all SRM algorithms, the zoom factor plays an important role on the accuracy of result. The key point of SRM is to determine the class labels of the fine spatial resolution pixels within the coarse spatial resolution pixel. For a given zoom factor z, there will be $z \times z$ fine spatial resolution pixels within the coarse spatial resolution pixel to be estimated. With the increase of z, the number of fine spatial resolution pixels would be increased exponentially, and more fine spatial resolution pixels within the coarse spatial resolution pixel need to be estimated. Therefore, the uncertainty of the estimation would be expected to increase, and the performance of the algorithm would decrease.

For the results of HC, as shown in Fig. 13 and Fig. 13, the land cover boundaries are jugged and many spatial details are missed. The Kappa and OA values of the results of HC, as shown in Table. I, stay at the lowest level. This is because that HC is based on the pixel scale, and does not consider the spatial distribution of classes at sub-pixel scale. By contrast, more land cover details at the sub-pixel scale are maintained by SRM including PS, SPA, BI, BP and the proposed learning-based SRM method. Visual comparison of the fine spatial resolution maps obtained from the various SRM analyses highlighted differences in the way they represented the land cover. For the results of PS, many land cover features are mapped as isolated rounded patches, and the spatial continuities are interrupted. This shortcoming becomes more serious with the increment of the zoom factor.

When $z = 8$, the Kappa and OA values of PS are 0.4739 and 0.6806, and are even lower than those of HC because the uncertainty of the fine spatial resolution pixel distributions in the resultant fine spatial resolution land cover map generated by PS is serious when the zoom factor is large. The fine spatial resolution land cover maps produced by SPA and BI visually differed from that obtained with PS with more spatial detail are maintained. The Kappa and OA values of fine spatial resolution land cover maps produced by SPA and BI are also higher than those of PS. However, numerous linear artifacts are found near the land cover boundaries in the obtained fine spatial resolution land cover maps produced by SPA and BI, and the linear artifacts become more serious with the increment of the zoom factor. The fine spatial resolution land cover maps produced by PS, SPA and BI are, therefore, less than ideal. This is because these SRM methods just apply the spatial dependence assumption to describe the land cover pattern, and this assumption will often be too simple to provide enough information for SRM in areas with complex land cover patterns.

Compared with the results of PS, SPA and BI, the linear artifacts in the results of BP are eliminated and the spatial continuities are maintained to some extent. The Kappa and OA values of the resultant fine spatial resolution land cover maps produced by BP at zoom factor of 5 and 8 are both higher than those of PS, SPA and BI. This improvement arises from the use of additional information about the spatial land cover pattern that is learned from the training database in the SRM procedure. However, in the resultant fine spatial resolution land cover maps produced by BP, many salt-and-pepper artifacts are found and many linear land cover features are also mapped as isolated small-sized patches. Moreover, with the increment of the zoom factor, the geometric integrity of features is more difficult to be maintained by the BP based SRM method. The shortcoming of the BP based SRM method is mainly caused by its two-step procedure and the impact of outliers during the learning procedure.

The resultant fine spatial resolution land cover maps produced by the proposed learning-based SRM method

are more similar to the reference (Fig. 7) at both zoom factors than the maps produced from the other SRM methods. Isolated land cover patches, jagged shapes and linear artifacts, which are common in the resultant fine spatial resolution land cover maps produced by aforementioned methods, are effectively eliminated by the proposed learning based SRM method. More spatial details, especially the linear features and the spatial land cover continuities are maintained. The Kappa and OA values of the resultant fine spatial resolution land cover maps produced by the proposed learning based SRM method are all the highest at both zoom factors.. Both the visual comparison and accuracy analysis indicate that the proposed learning-based SRM method is superior to the SRM algorithms used for comparison.

The test maps II to IV, as shown in Figs. 7(b) to (d), were used to further validate the performance of the proposed learning-based SRM method. As with the analyses focused on test map I, with the zoom factors of 5 and 8, the three fine spatial resolution test maps were degraded to produce the simulated coarse spatial resolution fraction images. These simulated coarse spatial resolution fraction images are then used as input to the SRM methods in order to produce the resultant fine spatial resolution land cover maps. The same parameter values used in the experiment of the test map I were applied for test maps II to IV. The resultant land cover maps produced by HC, PS, SPA, BI, BP and the proposed learning based SRM algorithm at zoom factors of 5 and 8 are all shown in Fig. 14 and Fig. 15, respectively. By using the original fine spatial resolution land cover maps as the reference, the accuracy analysis of three land cover maps at $z = 5$ and $z = 8$ are shown in Table II.

A similar trend as the experiment of the test map I is found by visually comparing the resultant fine spatial resolution land cover maps produced by different methods. The resultant land cover maps produced by HC have jagged boundaries and many spatial details are missed. By contrast, the fine spatial resolution land cover maps produced by SRM methods have smooth boundaries and more spatial details are maintained. The fine spatial resolution land cover maps produced by PS are locally smooth and many linear land cover features are mapped

into individual round patches for all three test maps. The spatial land cover pattern of the results produced by SPA and BI are much improved, however, numerous irregular linear artifacts exist near the boundaries. Moreover, more linear artifacts appear in the SPA and BI results of the test map III than those of the test map II and IV, due to the complex land cover features of the test map III, especially the urban class. The BP based SRM method can reconstruct more spatial details, and eliminate linear artifacts in the results of SPA and BI to some extent, due to additional spatial land cover information is learned from the extra fine spatial resolution land cover maps. However, many salt-and-pepper artifacts and isolated small-sized patches are still unavoidable due to the errors caused by the two-step process. By contrast, the fine spatial resolution land cover maps produced by the proposed learning-based SRM method, as shown in Fig. 14 and Fig. 15 at $z = 5$ and $z = 8$, are more similar to the reference fine spatial resolution land cover maps as shown in Fig. 7. The fine spatial resolution land cover maps produced by the proposed algorithm are smooth. Salt-and-pepper artifacts, isolated patches and irregular linear artifacts that appear in the results of some of the other SRM analyses are mostly eliminated. For all of the three testing land cover maps at both zoom factors of 5 and 8, more spatial detail, especially the linear features, are well maintained in the results of the proposed learning based SRM algorithm.
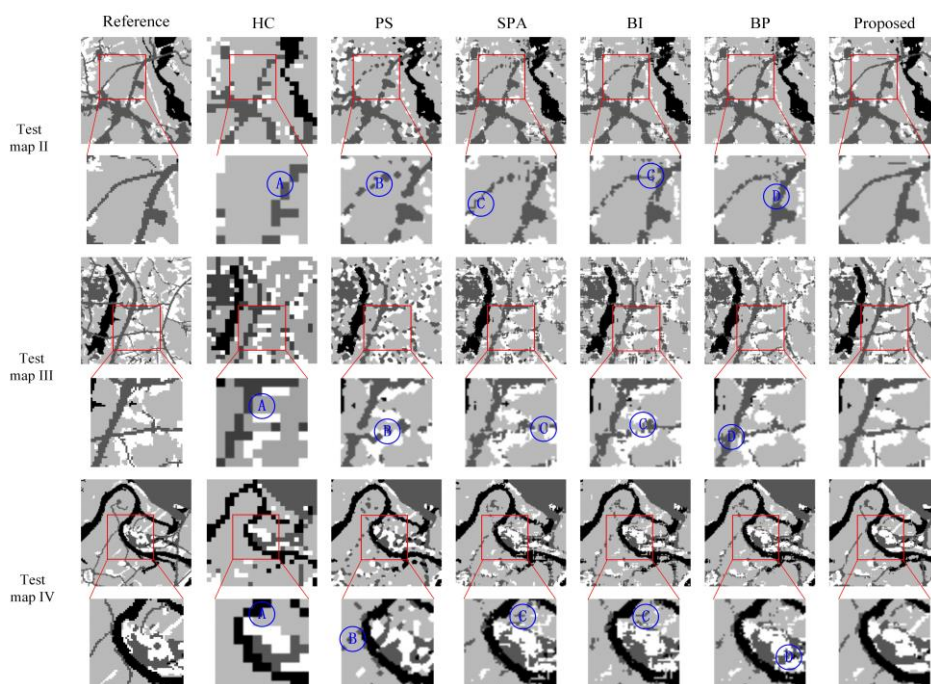
Fig. 14. Resultant land cover maps generated by different methods for test maps II-IV with $z = 5$. HC produces jagged boundaries (such as the area A); PS produces isolated patches (such as the area B); SPA and BI produce linear artifacts (such as the area C); and BP produces salt-and-pepper artifacts and isolated patches (such as the area D).
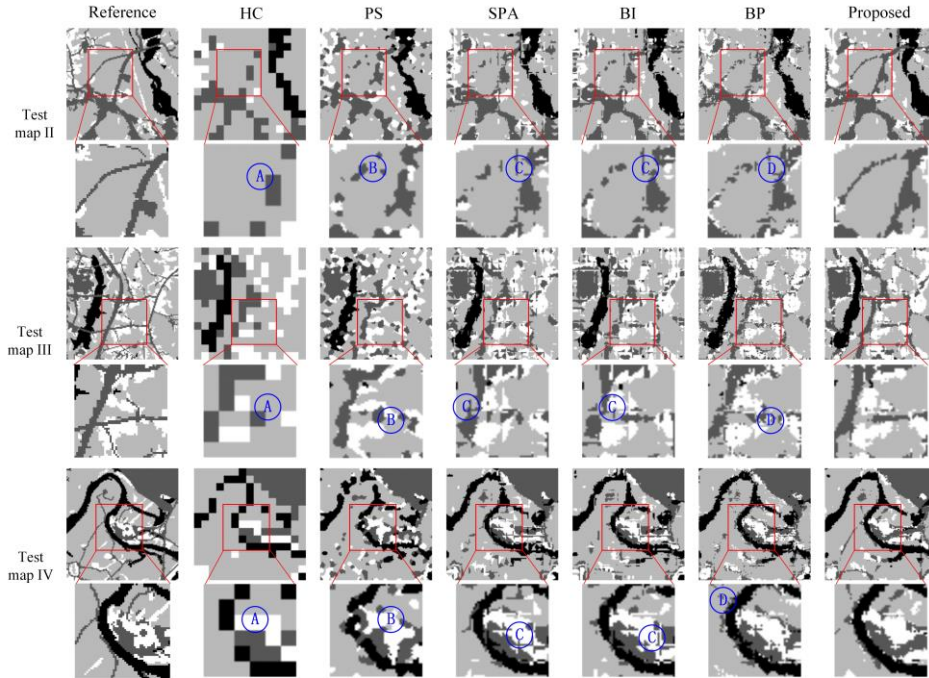

Fig. 15. Resultant land cover maps generated by different methods for test maps II-IV with $z = 8$. HC produces jagged boundaries (such as the area A); PS produces isolated patches (such as the area B); SPA and BI produce linear artifacts (such as the area C); and BP produces salt-and-pepper artifacts and isolated patches (such as the area D).

Table II. Kappa and Overall Accuracy (OA) values of the resultant land cover maps produced by different methods at $z = 5$ and $z = 8$ for test maps II-IV.

			HC	PS	SPA	BI	BP	Proposed
Test map II	z=5	Kappa	0.6576	0.7157	0.7466	0.7392	0.7465	0.7790
		OA	0.8126	0.8381	0.8556	0.8514	0.8556	0.8741
	z=8	Kappa	0.5746	0.5770	0.6190	0.6232	0.6230	0.6441
		OA	0.7690	0.7590	0.7829	0.7853	0.7852	0.7972
Test map III	z=5	Kappa	0.6006	0.6273	0.6547	0.6453	0.6596	0.6939
		OA	0.7481	0.7599	0.7776	0.7715	0.7808	0.8028
	z=8	Kappa	0.4922	0.4388	0.5027	0.5144	0.5033	0.5271

Test map IV		OA	0.6791	0.6385	0.6797	0.6872	0.6801	0.6954
	z=5	Kappa	0.6903	0.7592	0.7745	0.7802	0.7820	0.8131
		OA	0.8127	0.8503	0.8599	0.8634	0.8645	0.8838
	z=8	Kappa	0.6134	0.5972	0.6567	0.6677	0.6737	0.6863
		OA	0.7684	0.7497	0.7867	0.7935	0.7972	0.8051

The accuracy statistics of different methods for three testing land cover maps at zoom factors of 5 and 8 are shown in Table. II. When $z=5$, the Kappa and OA values of the results of HC are the lowest. It is also noted that both Kappa and OA values of the fine spatial resolution land cover maps produced by PS for three test maps are lower than those of HC at $z=8$, indicating that PS is inappropriate to be applied when zoom factor is large. For $z=5$ and $z=8$, the Kappa and OA values of the fine spatial resolution land cover maps produced by SPA and BI for three test maps almost stay at the same level. The Kappa values of the fine spatial resolution land cover maps produced by BP is higher than those of SPA and BI when $z=5$, however, there is no improvement of the Kappa and OA values when $z=8$. By contrast, the proposed learning based SRM algorithm produces the fine spatial resolution land cover maps with the highest Kappa and OA values, at both zoom factors of 5 and 8 for all three test maps, showing the advantage of the proposed learning-based SRM method.

IV. Discussions

The general principle for learning based SRM algorithms is that the spatial pattern of the estimated fine spatial resolution land cover map should be similar as that of existing fine spatial resolution land cover maps. The variation lies in the method used to represent the spatial land cover pattern. For the proposed learning based SRM algorithm, the assumption that a coarse spatial resolution mixed pixel patch with similar fractions has similar fine spatial resolution land cover pattern provides the basis for learning the prior spatial land cover pattern model. Noted that the similarity relationship only exists for patches, but is not applied for individual

coarse spatial resolution mixed pixel. The first reason is that the distribution of different land cover classes within a coarse spatial resolution pixel is always dependent with its surrounding coarse spatial resolution pixels. Secondly, determining the fine spatial resolution map within a coarse spatial resolution pixel one by one always leads to spatial discontinuity near coarse resolution pixel boundaries. By contrast, using patches can preserve the spatail continuity because these patches are overlapped.

Learning based SRM algorithms aim to make the estimated fine spatial resolution map similar with existing land cover maps. Therefore, how to measure their similarity is a key problem and different methods should lead to different SRM algorithms. In the proposed SRM algorithm, the similarity between two fine resolution land cover patches is computed by directly comparing their indicator maps. The objective function of the proposed SRM algorithm, as shown in equation (12), is then minimizing the difference between the estimated fine spatial resolution patch and corresponding fine spatial resolution patches. This objective function is indeed a spatially implicit model, as the spatial pattern is not represented by popular two-point statistics models, such as semi-variogram, but is directly represented by fine resolution patches themselves. Because the fine spatial resolution patch is a high dimensional vector, the effectiveness of similarity calculation should be further improved by extracting features from fine spatial resolution patches. Given the recent development of multiple point geo-statistics for spatial patterns reproduction [62], some approaches used to simulate spatial patterns in the multiple point geo-statistics community [63, 64] should be applied for the improvement of the proposed learning based SRM algorithm in the further research.

In the proposed learning based SRM algorithm, the spatial land cover pattern is represented by patch pairs generated class by class. For each land cover class, the indicator map only considers whether a fine spatial resolution pixel belongs to a certain land cover class or not, and does not differentiate other land cover classes any more. The inter-class relationship can be well presented by this method if only two land cover classes are

considered; however, more information about inter-class relationships is lost in indicator maps with the increment of land cover classes. In general, a patch often includes limited land cover classes and the inter-class relationship within a patch is not complex. Generating patch pairs class by class can then simplify the algorithm without losing too much inter-class information. In complex areas, however, considering the inter-class relationships of different land cover classes can provide additional information, and needs further study.

The selected neighboring patch pairs are crucial to the proposed learning based SRM algorithm. In order to ensure the quality of those neighboring patch pairs, they are chosen from the learning database with two threshold values at different scales. Threshold T_L indicates the difference of fraction values between patches at the coarse spatial resolution scale, and threshold T_h indicates the difference of indicator values between patches at the fine spatial resolution scale. Both of them play important roles on the performance of the proposed learning based SRM algorithm. From the experiment result, to be more specific, a relative large value of T_L and a relative small value of T_h are more likely to obtain fine spatial resolution land cover maps with higher accuracies. This implies that a good neighboring patch pair searching strategy is to start with a large number of candidate patch pairs and refine to a few best patch pair candidates. In practice, however, optimal values of T_L and T_h may differ between studies, and their values need to be optimized with the use of appropriate training samples. Automatic estimation of optimal threshold values could also be considered; however, it is a difficult issue and needs further study.

Table III. Computation time for different steps of the proposed SRM algorithm with zoom factors 5 and 8 for the test map I.

Zoom Factor	Building databases	Initial map Generation	Outlier rejection	Total
z = 5	183 s	776 s	785 s	1744 s
z = 8	129 s	473 s	619 s	1221 s

Program run time influences the application of the proposed learning based SRM algorithm. In the

experiments, the algorithm was tested on an Intel Core 5 Processor 3.20-GHz Duo CPU with 4 GB RAM using

MATLAB version 7.3. In general, building datasets and optimizing with the simulated annealing algorithm are

very time consuming. In the experiments, for building datasets, the number of patch pairs in the training database

is set to be 12×10^4. For the simulated annealing algorithm, the iteration number is set to be 1000 to ensure the

convergence. The iteration number is set to be 100 in outlier rejection, however, to enhance the computing

efficiency. With the aforementioned algorithm parameters and the implementation code without optimization,

the running time was shown in Table III. It is observed that the running time used for building databases is much

less than the initial map generation and outlier rejection steps, and less time is needed for a lower zoom factor.

V. Conclusions

In this paper, a novel learning based SRM algorithm was proposed and tested relative to a set of established

SRM methods. Compared with the simple spatial dependence prior model, the learning method can more

effectively describe the spatial land cover pattern, and make the resultant fine spatial resolution land cover map

more accurate. In the proposed learning based SRM algorithm, the spatial land cover pattern is represented by

the patch pairs, which include a fine spatial resolution patch and a coarse spatial resolution patch. The algorithm

first generates a learning database including a large amount of patch pairs. The K-D tree algorithm is used to

search neighboring patches for coarse spatial resolution patches in the input fraction images from the learning

database. These searched neighboring patches are used to estimate the latent fine spatial resolution land cover

map by solving an optimization problem, which aims to make the estimated fine spatial resolution land cover

map have similar spatial land cover pattern as these neighboring patches. Moreover, an iterative patch outlier

finding procedure is applied to reject outliers during the estimation procedure in order to enhance the result.

The performance of the proposed SRM algorithm was assessed with several experiments that used the

NLCD land cover maps as the reference. Some important parameters including the number of patch pairs in the

training database, the coarse spatial resolution scale fraction difference threshold value and the minimal fine

spatial resolution difference threshold value are discussed, and the optimal values are suggested according to the

experiment results. The proposed learning based SRM algorithm is also compared with several popular SRM

algorithms. The results shows that the proposed learning based SRM algorithm better maintains different land

cover patterns in all experiments. Notably, salt-and-pepper artifacts, isolated patches and irregular linear artifacts

that often appear in the resultant land cover maps produced by the popular SRM algorithms can be eliminated by

the proposed learning based SRM algorithm to a large extent. Moreover, the highest Kappa and overall accuracy

values are also derived by the proposed learning based algorithm.

Acknowledgements

References

[1]   P. M. Atkinson, "Issues of uncertainty in super-resolution mapping and their implications for the design of an
        inter-comparison study," *Int. J. Remote Sens.,* vol. 30, no. 20, pp. 5293-5308, 2009.

[2]   P. M. Atkinson, "Downscaling in remote sensing," *Int. J. Appl. Earth Obs. Geoinf.,* vol. 22, pp. 106-114, Jun,
        2013.

[3]   G. M. Foody, A. M. Muslim, and P. M. Atkinson, "Super-resolution mapping of the waterline from remotely
        sensed data," *Int. J. Remote Sens.,* vol. 26, no. 24, pp. 5381-5392, Dec, 2005.

[4]   F. Ling, F. Xiao, Y. Du, H. P. Xue, and X. Y. Ren, "Waterline mapping at the subpixel scale from remote
        sensing imagery with high-resolution digital elevation models," *Int. J. Remote Sens.,* vol. 29, no. 6, pp.
        1809-1815, 2008.

[5]   C. Huang, Y. Chen, and J. P. Wu, "DEM-based modification of pixel-swapping algorithm for enhancing
        floodplain inundation mapping," *Int. J. Remote Sens.,* vol. 35, no. 1, pp. 365-381, Jan, 2014.

[6]   A. M. Muad, and G. M. Foody, "Super-resolution mapping of lakes from imagery with a coarse spatial and
        fine temporal resolution," *Int. J. Appl. Earth Obs. Geoinf.,* vol. 15, pp. 79-91, Apr, 2012.

[7]   F. Ling, X. D. Li, F. Xiao, S. M. Fang, and Y. Du, "Object-based sub-pixel mapping of buildings
        incorporating the prior shape information from remotely sensed imagery," *Int. J. Appl. Earth Obs. Geoinf.,*
        vol. 18, pp. 283-292, 2012.

[8]   J. P. Ardila, V. A. Tolpekin, W. Bijker, and A. Stein, "Markov-random-field-based super-resolution mapping

for identification of urban trees in VHR images," *ISPRS J. Photogramm. Remote Sens.,* vol. 66, no. 6, pp. 762-775, 2011.

[9]   X. D. Li, Y. Du, and F. Ling, "Super-resolution mapping of forests with bitemporal different spatial resolution images based on the spatial-temporal markov random field," *IEEE J. Sel. Topics Appl. Earth Observ. Remote Sens.,* vol. 7, no. 1, pp. 29-39, Jan, 2014.

[10]   G. M. Foody, "The role of soft classification techniques in the refinement of estimates of ground control point location," *Photogramm. Eng. Remote Sens.,* vol. 68, no. 9, pp. 897-903, Sep, 2002.

[11]   X. D. Li, Y. Du, F. Ling, S. J. Wu, and Q. Feng, "Using a sub-pixel mapping model to improve the accuracy of landscape pattern indices," *Ecol. Indic.,* vol. 11, no. 5, pp. 1160-1170, 2011.

[12]   A. J. Tatem, H. G. Lewis, P. M. Atkinson, and M. S. Nixon, "Super-resolution target identification from remotely sensed images using a Hopfield neural network," *IEEE Trans. Geosci. Remote Sens.,* vol. 39, no. 4, pp. 781-796, 2001.

[13]   K. C. Mertens, L. P. C. Verbeke, E. I. Ducheyne, and R. R. De Wulf, "Using genetic algorithms in sub-pixel mapping," *Int. J. Remote Sens.,* vol. 24, no. 21, pp. 4241-4247, Nov, 2003.

[14]   P. M. Atkinson, "Sub-pixel target mapping from soft-classified remotely sensed imagery," *Photogramm. Eng. Remote Sens.,* vol. 71, no. 7, pp. 839-846, Jul, 2005.

[15]   T. Kasetkasem, M. K. Arora, and P. K. Varshney, "Super-resolution land cover mapping using a Markov random field based approach," *Remote Sens. Environ.,* vol. 96, no. 3-4, pp. 302-314, Jun, 2005.

[16]   A. Boucher, and P. C. Kyriakidis, "Super-resolution land cover mapping with indicator geostatistics," *Remote Sens. Environ.,* vol. 104, no. 3, pp. 264-282, Oct, 2006.

[17]   Y. Gu, Y. Zhang, and J. Zhang, "Integration of spatial-spectral information for resolution enhancement in hyperspectral images," *IEEE Trans. Geosci. Remote Sens.,* vol. 46, no. 5, pp. 1347-1358, May, 2008.

[18]   Y. Ge, S. Li, and V. C. Lakhan, "Development and testing of a subpixel mapping algorithm," *IEEE Trans. Geosci. Remote Sens.,* vol. 47, no. 7, pp. 2155-2164, Jul, 2009.

[19]   A. Villa, J. Chanussot, J. A. Benediktsson, and C. Jutten, "Spectral unmixing for the classification of hyperspectral images at a finer spatial resolution," *IEEE J. Sel. Top. Signal Process.,* vol. 5, no. 3, pp. 521-533, Jun, 2011.

[20]   A. M. Muad, and G. M. Foody, "Impact of land cover patch size on the accuracy of patch area representation in HNN-based super resolution mapping," *IEEE J. Sel. Topics Appl. Earth Observ. Remote Sens.,* vol. 5, no. 5, pp. 1418-1427, Oct, 2012.

[21]   Y. F. Su, G. M. Foody, A. M. Muad, and K. S. Cheng, "Combining pixel swapping and contouring methods to enhance super-resolution mapping," *IEEE J. Sel. Topics Appl. Earth Observ. Remote Sens.,* vol. 5, no. 5, pp. 1428-1437, Oct, 2012.

[22]   Q. M. Wang, L. G. Wang, and D. F. Liu, "Particle swarm optimization-based sub-pixel mapping for remote-sensing imagery," *Int. J. Remote Sens.,* vol. 33, no. 20, pp. 6480-6496, 2012.

[23]   Y. Ge, "Sub-pixel land-cover mapping with improved fraction images upon multiple-point simulation," *Int. J. Appl. Earth Obs. Geoinf.,* vol. 22, pp. 115-126, Jun, 2013.

[24]   X. H. Tong, X. Zhang, J. Shan, H. Xie, and M. L. Liu, "Attraction-repulsion model-based subpixel mapping of multi-/hyperspectral imagery," *IEEE Trans. Geosci. Remote Sens.,* vol. 51, no. 5, pp. 2799-2814, May, 2013.

[25]   Q. M. Wang, W. Z. Shi, and L. G. Wang, "Allocating classes for soft-then-hard subpixel mapping algorithms in units of class," *IEEE Trans. Geosci. Remote Sens.,* vol. 52, no. 5, pp. 2940-2959, May, 2014.

[26]   Y. H. Zhang, Y. Du, X. D. Li, S. M. Fang, and F. Ling, "Unsupervised subpixel mapping of remotely sensed imagery based on fuzzy c-means clustering approach," *IEEE Geosci. Remote Sens. Lett.,* vol. 11, no. 5, pp.

1024-1028, May, 2014.

[27] Y. F. Zhong, and L. P. Zhang, "Remote sensing image subpixel mapping based on adaptive differential evolution," *IEEE Trans. Syst. Man Cybern. Part B-Cybern.,* vol. 42, no. 5, pp. 1306-1329, Oct, 2012.

[28] F. Ling, X. D. Li, F. Xiao, and Y. Du, "Superresolution land cover mapping using spatial regularization," *IEEE Trans. Geosci. Remote Sens.,* vol. 52, no. 7, pp. 4424-4439, Jul, 2014.

[29] K. C. Mertens, B. De Baets, L. P. C. Verbeke, and R. R. De Wulf, "A sub-pixel mapping algorithm based on sub-pixel/pixel spatial attraction models," *Int. J. Remote Sens.,* vol. 27, no. 15, pp. 3293-3310, Aug, 2006.

[30] F. Ling, X. D. Li, Y. Du, and F. Xiao, "Sub-pixel mapping of remotely sensed imagery with hybrid intra- and inter-pixel dependence," *Int. J. Remote Sens.,* vol. 34, no. 1, pp. 341-357, 2013.

[31] X. D. Li, Y. Du, F. Ling, Q. Feng, and B. T. Fu, "Superresolution mapping of remotely sensed image based on Hopfield neural network with anisotropic spatial dependence model," *IEEE Geosci. Remote Sens. Lett.,* vol. 11, no. 7, pp. 1265-1269, Jul, 2014.

[32] M. W. Thornton, P. M. Atkinson, and D. A. Holland, "A linearised pixel-swapping method for mapping rural linear land cover features from fine spatial resolution remotely sensed imagery," *Comput. Geosci.,* vol. 33, no. 10, pp. 1261-1272, Oct, 2007.

[33] F. Ling, Y. Du, X. D. Li, Y. H. Zhang, F. Xiao, S. M. Fang, and W. B. Li, "Superresolution land cover mapping with multiscale information by fusing local smoothness prior and downscaled coarse fractions," *IEEE Trans. Geosci. Remote Sens.,* vol. 52, no. 9, pp. 5677-5692, Sep, 2014.

[34] G. M. Foody, "Sharpening fuzzy classification output to refine the representation of sub-pixel land cover distribution," *Int. J. Remote Sens.,* vol. 19, no. 13, pp. 2593-2599, Sep, 1998.

[35] M. Q. Nguyen, P. M. Atkinson, and H. G. Lewis, "Superresolution mapping using a Hopfield neural network with fused images," *IEEE Trans. Geosci. Remote Sens.,* vol. 44, no. 3, pp. 736-749, Mar, 2006.

[36] X. D. Li, F. Ling, Y. Du, and Y. H. Zhang, "Spatially adaptive superresolution land cover mapping with multispectral and panchromatic images," *IEEE Trans. Geosci. Remote Sens.,* vol. 52, no. 5, pp. 2810-2823, May, 2014.

[37] M. Q. Nguyen, P. M. Atkinson, and H. G. Lewis, "Super-resolution mapping using Hopfield neural network with panchromatic imagery," *Int. J. Remote Sens.,* vol. 32, no. 21, pp. 6149-6176, 2011.

[38] A. Robin, S. Le Hegarat-Mascle, and L. Moisan, "Unsupervised subpixelic classification using coarse-resolution time series and structural information," *IEEE Trans. Geosci. Remote Sens.,* vol. 46, no. 5, pp. 1359-1374, May, 2008.

[39] M. Q. Nguyen, P. M. Atkinson, and H. G. Lewis, "Superresolution mapping using a Hopfield neural network with LIDAR data," *IEEE Geosci. Remote Sens. Lett.,* vol. 2, no. 3, pp. 366-370, Jul, 2005.

[40] P. Aplin, and P. M. Atkinson, "Sub-pixel land cover mapping for per-field classification," *Int. J. Remote Sens.,* vol. 22, no. 14, pp. 2853-2858, Sep, 2001.

[41] F. Ling, Y. Du, F. Xiao, H. P. Xue, and S. J. Wu, "Super-resolution land-cover mapping using multiple sub-pixel shifted remotely sensed images," *Int. J. Remote Sens.,* vol. 31, no. 19, pp. 5023-5040, 2010.

[42] L. G. Wang, and Q. M. Wang, "Subpixel mapping using markov random field with multiple spectral constraints from subpixel shifted remote sensing images," *IEEE Geosci. Remote Sens. Lett.,* vol. 10, no. 3, pp. 598-602, May, 2013.

[43] X. Xu, Y. F. Zhong, L. P. Zhang, and H. Y. Zhang, "Sub-pixel mapping based on a MAP model with multiple shifted hyperspectral imagery," *IEEE J. Sel. Topics Appl. Earth Observ. Remote Sens.,* vol. 6, no. 2, pp. 580-593, Apr, 2013.

[44] X. Xu, Y. F. Zhong, and L. P. Zhang, "A sub-pixel mapping method based on an attraction model for multiple shifted remotely sensed images," *Neurocomputing,* vol. 134, pp. 79-91, Jun, 2014.

[45]   Q. M. Wang, and W. Z. Shi, "Utilizing multiple subpixel shifted images in subpixel mapping with image interpolation," *IEEE Geosci. Remote Sens. Lett.,* vol. 11, no. 4, pp. 798-802, Apr, 2014.

[46]   F. Ling, W. B. Li, Y. Du, and X. D. Li, "Land cover change mapping at the subpixel scale with different spatial-resolution remotely sensed imagery," *IEEE Geosci. Remote Sens. Lett.,* vol. 8, no. 1, pp. 182-186, 2011.

[47]   Y. Xu, and B. Huang, "A spatio-temporal pixel-swapping algorithm for subpixel land cover mapping," *IEEE Geosci. Remote Sens. Lett.,* vol. 11, no. 2, pp. 474-478, Feb, 2014.

[48]   A. J. Tatem, H. G. Lewis, P. M. Atkinson, and M. S. Nixon, "Super-resolution land cover pattern prediction using a Hopfield neural network," *Remote Sens. Environ.,* vol. 79, no. 1, pp. 1-14, Jan, 2002.

[49]   A. Boucher, P. C. Kyriakidis, and C. Cronkite-Ratcliff, "Geostatistical solutions for super-resolution land cover mapping," *IEEE Trans. Geosci. Remote Sens.,* vol. 46, no. 1, pp. 272-283, Jan, 2008.

[50]   H. Jin, G. Mountrakis, and P. Li, "A super-resolution mapping method using local indicator variograms," *Int. J. Remote Sens.,* vol. 33, no. 24, pp. 7747-7773, 2012.

[51]   K. C. Mertens, L. P. Verbeke, and R. Wulf, "Sub-pixel mapping with neural networks: real-world spatial configurations learned from artificial shapes," *Proceedings of 4th International Symposium on Remote Sensing of Urban Areas (Regensburg, Germany)*, pp. 117-121, 2003.

[52]   L. Wang, Y. Zhang, and J. Li, "BP neural network based Sub-pixel mapping method," *Intelligent Computing in Signal Processing and Pattern Recognition*, pp. 755-760, 2006.

[53]   L. Zhang, K. Wu, Y. Zhong, and P. Li, "A new sub-pixel mapping algorithm based on a BP neural network with an observation model," *Neurocomputing,* vol. 71, no. 10-12, pp. 2046-2054, 2008.

[54]   K. Wu, L. Zhang, R. Niu, B. Du, and Y. Wang, "Super-resolution land-cover mapping based on the selective endmember spectral mixture model in hyperspectral imagery," *Opt. Eng.,* vol. 50, no. 12, pp. 126201, 2011.

[55]   Y. H. Zhang, Y. Du, F. Ling, S. M. Fang, and X. D. Li, "Example-based super-resolution land cover mapping using support vector regression," *IEEE J. Sel. Topics Appl. Earth Observ. Remote Sens.,* vol. 7, no. 4, pp. 1271-1283, Apr, 2014.

[56]   F. Ling, Y. Du, X. D. Li, W. B. Li, F. Xiao, and Y. H. Zhang, "Interpolation-based super-resolution land cover mapping," *Remote Sens. Lett.,* vol. 4, no. 7, pp. 629-638, Jul, 2013.

[57]   W. T. Freeman, T. R. Jones, and E. C. Pasztor, "Example-based super-resolution," *Computer Graphics and Applications, IEEE,* vol. 22, no. 2, pp. 56-65, 2002.

[58]   J. L. Bentley, "Multidimensional binary search trees used for associative searching," *Communications of the ACM,* vol. 18, no. 9, pp. 509-517, 1975.

[59]   V. A. Tolpekin, and A. Stein, "Quantification of the effects of land-cover-class spectral separability on the accuracy of Markov-random-field-based superresolution mapping," *IEEE Trans. Geosci. Remote Sens.,* vol. 47, no. 9, pp. 3283-3297, 2009.

[60]   G. Xian, C. Homer, and J. Fry, "Updating the 2001 National Land Cover Database land cover classification to 2006 by using Landsat imagery change detection methods," *Remote Sens. Environ.,* vol. 113, no. 6, pp. 1133-1147, Jun, 2009.

[61]   Y. Makido, A. Shortridge, and J. P. Messina, "Assessing alternatives for modeling the spatial distribution of multiple land-cover classes at sub-pixel scales," *Photogramm. Eng. Remote Sens.,* vol. 73, no. 8, pp. 935-943, Aug, 2007.

[62]   G. Mariethoz, and S. Lefebvre, "Bridges between multiple-point geostatistics and texture synthesis: Review and guidelines for future research," *Comput. Geosci.,* vol. 66, pp. 66-80, May, 2014.

[63]   M. Honarkhah, and J. Caers, "Direct pattern-based simulation of non-stationary geostatistical models," *Math. Geosci.,* vol. 44, no. 6, pp. 651-672, Aug, 2012.

[64]   M. Honarkhah, and J. Caers, "Stochastic simulation of patterns using distance-based pattern modeling," *Math. Geosci.,* vol. 42, no. 5, pp. 487-517, Jul, 2010.